RESEARCH ARTICLE

The Unconventional Cadmium Borosulfates Cd[B₂O(SO₄)₃] and Cd₄[B₂O(SO₄)₆]

Matthias Hämmer[a] and Henning A. Höppe*[a]

Herrn Prof. Dr. Wolfgang Schnick zum 65. Geburtstag gewidmet.

Borosulfates are an expanding class of silicate-analogous materials. We report the syntheses and crystal structures of two unconventional cadmium borosulfates. $Cd[B_2O(SO_4)_3]$ crystallises in a new structure type in space group *Pnma* (no. 62, $a = 896.92(8)$, $b = 1152.0(1)$, $c = 872.75(8)$ pm, 1380 refl., 94 ref. param., $wR_2 = 0.112$). $Cd_4[B_2O(SO_4)_6]$ adapts the α-$Mg_4[B_2O(SO_4)_6]$-type structure with space group $P\bar{3}$ (no. 147, $a = 822.22(4)$, $c = 797.88(5)$ pm, 1810 refl., 58 ref. param., $wR_2 = 0.078$). Together with simultaneously elsewhere reported conventional phyllosilicate-analogous $Cd[B_2(SO_4)_4]$, there are now in total three cadmium borosulfates with differing dimensionality of their anions, i.e. 0D, 1D and 2D. These results highlight the special position of cadmium in the periodic table and the

ambiguity of its behaviour as main group or transition metal when comparing to other analogous or related borosulfates. The $[B_2O(SO_4)_3]^{2-}$ and $[B_2O(SO_4)_6]^{8-}$ anions are known from other main group and transition metal borosulfates. However, Cd^{2+} is the first cation for which borosulfates comprising both anions are reported for the same cation. Moreover, the optical and thermal properties of both compounds are reported using IR and UV-Vis spectroscopy as well as thermogravimetry. Both unconventional borosulfates were prepared by the thermal decomposition of the conventional borosulfate $Cd[B_2(SO_4)_4]$ pursueing our studies on the complex thermal decomposition behaviour of such borosulfates.

Introduction

Borosulfates are a fast-growing class of silicate-analogous materials.[1] Despite the first crystal structure being reported as recently as 2012[2] there are over 70 borosulfates with known crystal structure up to date.[3] Borosulfates can be classified as silicate-analogous in two ways: Firstly, they comprise – with rare exceptions showing trigonal planar coordinated boron[4,5] – exclusively corner sharing borate and sulfate tetrahedra. Secondly, these structures can be considered to comprise supertetrahedra TX_4 formed by a boron atom acting as centre T coordinated tetrahedrally by four SO_4 moieties X as frequently observed in the building unit $[B(SO_4)_4]^{5-}$. Then, borosulfates can be classified by the dimensionality of their anion, i.e. the connection of supertetrahedra. For that, Friedrich Liebau's classification of silicates is adapted.[6] Accordingly, a silicate-analogous compound like the cadmium nitridophosphate Cd-

$[P_2N_4]$ containing PN_4 tetrahedra is expected to form a tectosilicate anion, which is indeed the case.[7]

Beyond conventional borosulfates exhibiting exclusively B—O—S bonds within the anion there are also several so-called unconventional borosulfates featuring B—O—B bridges as reported for $Mg_4[B_2O(SO_4)_6]$[8] or S—O—S bridges found for instance in $Sr[B_2(SO_4)_3(S_2O_7)]$[9] formally violating Loewenstein's rule[10] and Pauling's fourth rule, respectively.[11]

In general, the formation of S—O—S, exclusively B—O—S and B—O—B bridges in borosulfates is governed by the SO_3 content during the solvothermal syntheses.[9,12] The majority of unconventional borosulfates of divalent metal cations with B—O—B bridges adapt either $M[B_2O(SO_4)_3]$ or $M_4[B_2O(SO_4)_6]$ as formula in which the special topology is reflected; in $Sr[B_3O(SO_4)_4(SO_4H)]$ even three borate tetrahedra share common vertices,[13] a motif better known from nitridosilicates. So far, for each divalent metal cation only one of both compositions is known: $M[B_2O(SO_4)_3]$ (M = Sr, Ba, Pb)[14,15] and $M_4[B_2O(SO_4)_6]$ (M = Mg, Mn, Co, Ni, Zn).[8] However, compounds with both types of sum formulae are presented in this work for divalent cadmium for the first time.Coevally, we report the first cadmium borosulfates $Cd[B_2(SO_4)_4]$,[16] a phyllosilicate-analogous borosulfates crystallising in the $Mn[B_2(SO_4)_4]$-type structure.[17]

The element cadmium belongs to the zinc group of the periodic table – usually called group 12 or group IIB. The latter nomenclature highlights the ambiguity of this group. Despite this group being part of the transition metals in the most common 18-column version of the periodic table zinc, cadmium and mercury should rather be considered main group metals due to the lack of valence d electrons. The location of the zinc group was part of many elaborate discussion in literature.[18,19]

[a] *Dr. M. Hämmer, Prof. Dr. H. A. Höppe*
Lehrstuhl für Festkörperchemie, Institut für Physik
Universität Augsburg
Universitätsstraße 1, 86159 Augsburg, Germany
E-mail: henning@ak-hoeppe.de

Sanderson's double appendix periodic table locates cadmium next to strontium and the zinc group below magnesium.[19] This localisation was abandoned in the 18-column version mainly due to symmetric reasons. However, this already demonstrated the janiform behaviour of cadmium.

The borosulfates $Cd[B_2O(SO_4)_3]$ and $Cd_4[B_2O(SO_4)_6]$, whose syntheses, crystal structures and optical and thermal properties are reported in this work, together with the simultaneously reported $Cd[B_2(SO_4)_4]$ are good examples to consolidate this aspect since the adapted crystal structures and their relationship to analogous main group and transition metal borosulfates highlights the ambiguity discussed above.

Results and Discussion

Syntheses

Both, $Cd[B_2O(SO_4)_3]$ and $Cd_4[B_2O(SO_4)_6]$ were prepared as colourless, coarsely crystalline powders containing single-crystals via the thermal decomposition of $Cd[B_2(SO_4)_4]$. The solvothermal synthesis of the latter was reported elsewhere.[16] For $Cd[B_2O(SO_4)_3]$, $Cd[B_2(SO_4)_4]$ was heated in ambient atmosphere at 250 °C for 24 h. Powder XRD and Rietveld refinement confirmed the formation of $Cd[B_2O(SO_4)_3]$ with a 2 wt.% $CdSO_4$ side phase (Figure 1 and table S1). The preparation of $Cd_4[B_2O(SO_4)_6]$ is complicated due to the simultaneous former process and the formation of $CdSO_4$ – as discussed in detail with the thermal properties below. The smallest $CdSO_4$ side phase of 11 wt.% according to Rietveld refinement (Figure S1) was observed when heating $Cd[B_2(SO_4)_4]$ under ambient atmosphere at 300 °C for 2 h. Details can be found in the experimental section.

While the preparation of $M[B_2O(SO_4)_3]$ ($M=$ Sr, Ba) via the thermal decomposition of $M[B_2(SO_4)_4]$ is well known,[9,12] $Cd_4[B_2O(SO_4)_6]$ is the first member of the $M_4[B_2O(SO_4)_6]$ group for which this synthesis path was observed.

Crystal Structures

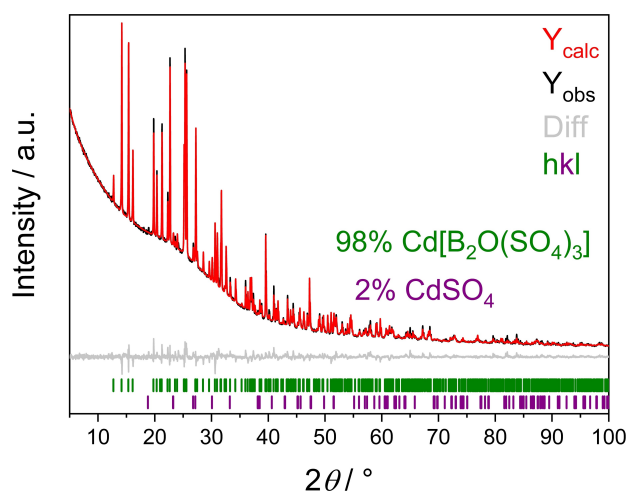$Cd[B_2O(SO_4)_3]$ crystallises in a new structure type orthorhombically with space group *Pnma* (no. 62) and four formula units per unit cell (Figure 2). Details can be found in Tables 1 and S2. The one-dimensional anion comprises sulfate and borate tetrahedra and both B–O–S as well as B–O–B bridges. Therefore, this borosulfate can be classified as unconventional. The anion forms loop branched *zweier* double chains comprising the fundamental building unit $[B_2O(SO_4)_3]^{2-}$ along [100] (Figure 3). The boron-oxygen and sulfur-oxygen distances ranging from 142 to 149 pm and from 142 to 152 pm are in line with the sum of the respective ionic radii (146 pm and 147 pm)[20] with the shortest B–O distance towards the oxygen atom shared by two borate groups and the longest S–O distances towards corner-sharing borate tetrahedra both due to electrostatic reasons. Two borate and one sulfate group form *dreier* rings as part of the chain-shaped borosulfate anion (Figure S2). The deviations from the tetrahedral symmetry Δ_{tetr} were calculated by the method of Balić-Žunić and Makovicky based on all ligands
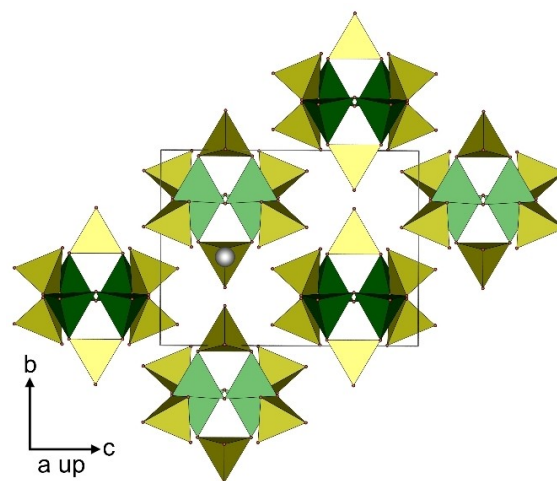

Figure 2. Unit cell of $Cd[B_2O(SO_4)_3]$: cadmium atoms are grey, borate tetrahedra green, sulfate tetrahedra yellow, oxygen atoms red.
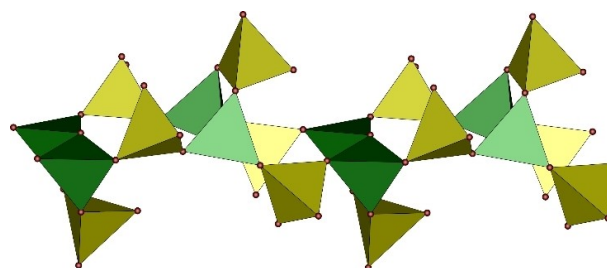
Figure 3. Part of the chains in $Cd[B_2O(SO_4)_3]$ running along [100] viewed almost along [001]; the sulfate groups that are part of the *dreier* ring together with two borate tetrahedra point both towards the top and the bottom of this representation; borate tetrahedra green, sulfate tetrahedra yellow, oxygen atoms red.

Figure 1. Rietveld-Refinement of the $Cd[B_2O(SO_4)_3]$ sample; further details can be found in Table S1.

Table 1. Crystal data and structure refinements of $Cd[B_2O(SO_4)_3]$ and $Cd_4[B_2O(SO_4)_6]$ determined from single crystal X-ray diffraction.[a]

	$Cd[B_2O(SO_4)_3]$	$Cd_4[B_2O(SO_4)_6]$
CSD–No.	2177540	2177539
M/g mol^{-1}	438.20	1063.58
crystal size/mm^3	$0.10 \times 0.07 \times 0.05$	$0.15 \times 0.09 \times 0.07$
temperature/K	250(2)	250(2)
space group	$Pnma$ (no. 62)	$P\bar{3}$ (no. 147)
a/pm	896.92(8)	822.22(4)
b/pm	1152.0(1)	
c/pm	872.75(8)	797.88(5)
volume/10^6 pm^3	901.79(14)	467.14(5)
Z	4	1
ρ_{calcd}/g cm^{-3}	3.23	3.78
absorption coefficient μ/mm^{-1}	3.20	5.30
$F(000)$/e	840	498
radiation; wavelength λ/Å		MoK_α; 0.71073
diffractometer		Bruker D8 Venture
θ range/°	2.93–30.00	3.84–42.47
absorption correction		multi-scan
transmission (min; max)	0.625; 0.748	0.606; 0.752
index range $h\|k\|l$	$\pm 12\|\pm 16\|\pm 12$	$-9/+11\|-15/+10\|-10/+13$
reflections collected	13147	2421
independent reflections	1380	1810
obs. reflections ($I > 2\,\sigma(I)$)	1329	1585
refined parameters	94	59
R_{int}	0.045	0.032
R_1	0.044	0.034
wR_2	0.112	0.073
GooF	1.427	1.081
residual electron density (max; min)/e^- Å^{-3}	1.06; −1.85	1.00; −1.44

[a] The respective standard deviations are given in parentheses.

enclosing spheres on experimental data.[21,22] The borate and sulfate tetrahedra can be considered regular[23] with deviations of 0.17% and 0.02 to 0.13%, respectively. The $[B_2O(SO_4)_3]^{2-}$ anion was so far only found for the heavy main group metal borosulfates $M[B_2O(SO_4)_3]$ ($M =$ Sr, Ba, Pb).[14,15] These adapt two structure types ($Ba[B_2O(SO_4)_3]$ and $Pb[B_2O(SO_4)_3]$) related by a common supergroup.[15] Both comprise unconventional inosilicate-analogous borosulfate anions very similar to $Cd[B_2O(SO_4)_3]$. In contrast, all sulfate tetrahedra that are part of the *dreier* rings point along the same direction in $M[B_2O(SO_4)_3]$ ($M =$ Sr, Ba, Pb), but are bidirectional in $Cd[B_2O(SO_4)_3]$ (Figure 3). Further, the propagation direction of the anionic chains is alternating along c and not changed along b (Figure 2) similar to $Pb[B_2O(SO_4)_3]$ and in contrast to $M[B_2O(SO_4)_3]$ ($M =$ Sr, Ba) where the direction is changed in both directions perpendicular to the chain.[14,15]

Between the chains Cd^{2+} cations are situated and coordinated by seven oxygen atoms stemming from six monodentate sulfate groups and two monodentate borate groups (Figure S3). The latter share one oxygen atom that coordinates the cadmium cation. Coordinating oxygen atoms stemming from borate tetrahedra are rare in borosulfates.[15,24] The coordination can be described as a distorted monocapped trigonal prism (Figure S3). The interatomic distances range from 227 to 241 pm agree well with the sum of the ionic radii (238 pm).[20] The longest cadmium-oxygen distance is observed for the

oxygen atom bridging the two borate groups due to sterical reasons.

In contrast, the cations in $M[B_2O(SO_4)_3]$ ($M =$ Sr, Ba, Pb) are tetracapped trigonal prismatically coordinated.[14,15] This is either enabled by or the reason for the smaller spread of the anionic chains discussed above.

Due to the different orientation of the sulfate groups that are part of the *dreier* ring, i.e. monodirectional for $M[B_2O(SO_4)_3]$ ($M =$ Sr, Ba, Pb) and bidirectional for $Cd[B_2O(SO_4)_3]$, there is no group-subgroup relation between the former and the latter crystal structures despite the same topology within the borosulfate anion. However, the difference in the cations' ionic radii is large.

$Cd_4[B_2O(SO_4)_6]$ crystallises trigonally in space group $P\bar{3}$ (no. 147) with one formula unit per unit cell (Figure 4) and adapts the structure type of α-$Mg_4[B_2O(SO_4)_6]$.[8] Details can be found in Tables 1 and S3. The unconventional zero-dimensional borosulfate anion comprises dimeric open-branched quadruple tetrahedra $\{oB,4 \text{ t}\}[B_2O(SO_4)_6]^{8-}$ (Figure S4). The dimeric corner-sharing B_2O_7 backbone featuring a linear B–O–B bridge – also violating Loewenstein's rule – is satured by six sulfate tetrahedra. The boron-oxygen and sulfur-oxygen distances range from 135 to 151 pm and 145 to 151 pm. Thus, they are in agreement with sum of the respective ionic radii (146 pm and

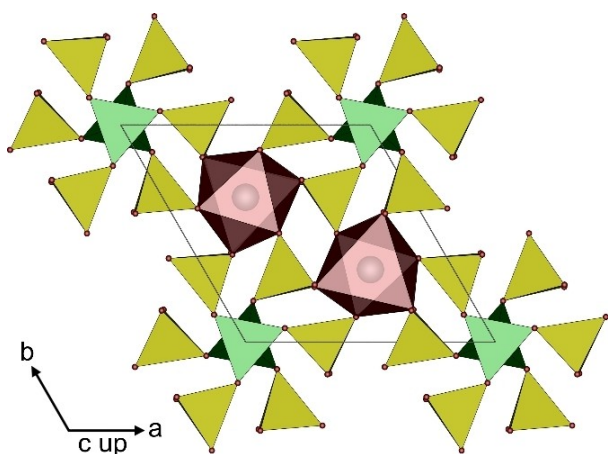**Figure 4.** Unit cell of $Cd_4[B_2O(SO_4)_6]$: cadmium atoms are grey, borate tetrahedra green, sulfate tetrahedra yellow, oxygen atoms red, CdO_6 octahedra semitransparent red.

147 pm). The shortest B–O distance occurs within the B–O–B bridge. This is also the case in $Cd[B_2O(SO_4)_3]$ discussed above. The distance is significantly smaller in $Cd_4[B_2O(SO_4)_6]$ – the simple reason is that presumably an unresolved vibration perpendicular to the linear B–O–B linkage supported by a slightly larger displacement parameter. The longest boron-oxygen and sulfur-oxygen distances are found as part of the B–O–S bridges. Again, both are observed due to electrostatic reasons. The borate and sulfate tetrahedra can be considered regular[23] with deviations[21,22] of 0.12 % and 0.09 %, respectively.

Charge balance is achieved by Cd^{2+} cations octahedrally coordinated by six oxygen atoms stemming from six monodentate sulfate groups (Figure S5). There are two crystallographically independent cadmium atoms. The CdO_6 octahedra form Cd_2O_9 dimers via face sharing (Figure 5) that are connected to the borosulfate anion resulting in a network. The interatomic distances range between 219 and 234 pm in agreement with the sum of the ionic radii (238 pm).[20] Additionally, the deviations from the octahedral symmetry Δ_{oct} as well as distance of the cadmium atoms from the centroids of the octahedra were calculated by the method of Balić-Žunić and
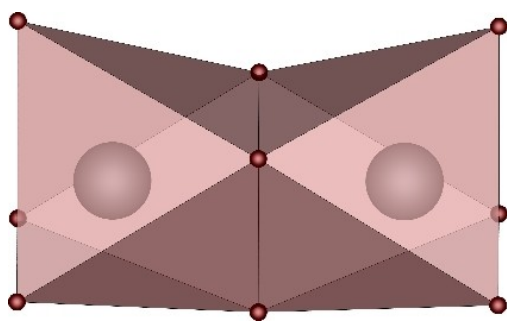

Figure 5. Cd_2O_9 dimers formed by face sharing of two CdO_6 octahedra in $Cd_4[B_2O(SO_4)_6]$; cadmium atoms grey, oxygen atoms red.

Makovicky[21,22] for the CdO_6 octahedra. While the octahedra deviate only slightly with deviations of 2.6 and 2.3 % the two cadmium atoms deviate from the centroid of the octahedron by 10 and 12 pm, respectively, due to electrostatic repulsion. This yields a cadmium-cadmium distance of 337 pm. This is the largest M–M distance for all known borosulfates adapting the bk;α-$Mg_4[B_2O(SO_4)_6]$ structure type; this coincides with the simple fact that divalent cadmium is the largest cation successfully incorporated in this type of borosulfate so far.

Both title compounds contain B–O–B bridges with boron saturated with three sulfate tetrahedra each; considering this feature by formally replacing sulfate by X and boron by T to recognise similiarities to silicates easier this yields a T_2X_6 unit and resembles the arrangement of a reduced silicate like in $Sr[Si_6N_8]$ featuring a T–T bond.[25]

The formation of both $Cd[B_2O(SO_4)_3]$ and $Cd_4[B_2O(SO_4)_6]$ highlights the janiform behaviour of cadmium iridescent between alkaline-earth and transition metal as mentioned in the introduction. When including $Cd[B_2(SO_4)_4]$[16] in the discussion cadmium behaves similar to magnesium and the transition metals manganese, cobalt, nickel, and zinc in the cases of $Cd_4[B_2O(SO_4)_6]$ and $Cd[B_2(SO_4)_4]$ and similar to the heavier main group metals strontium, barium and lead in the case of $Cd[B_2O(SO_4)_3]$. In the first two cases, the ionic radius of cadmium is closer to the respective metals than the last case explaining why isotypic or homeotypic versus only similar structures are adapted, respectively.

Electrostatic Calculations

The electrostatic reasonability of the crystal structures of $Cd[B_2O(SO_4)_3]$ and $Cd_4[B_2O(SO_4)_6]$ and all coordination numbers were confirmed by calculations based on the MAPLE (MAdelung Part of Lattice Energy) concept (Tables S4).[26]

Optical Properties

The **infrared spectrum** of $Cd[B_2O(SO_4)_3]$ is shown in Figure 6 in the regime of 1400–400 cm^{-1} (full spectra in Figure S6). This is the crucial part of the spectrum containing the respective vibrations related to boron and sulfur centred oxygen tetrahedra. The vibrations can be assigned in line with earlier results on borosulfates.[4,8,15] The asymmetric S–O stretching vibrations range from 1350 to 1240 cm^{-1} and are followed by the B–O stretching bands between 1180 and 970 cm^{-1}. B–O–B bending vibrations are found at 910 cm^{-1}. The symmetric S–O stretching vibrations are present in form of the broad band around 830 cm^{-1}. Below the spectrum is governed by O–S–O, O–B–O and S–O–B bending vibrations.

In the case of $Cd_4[B_2O(SO_4)_6]$, the interpretation of the IR spectrum (Figure S7) is complicated by the $CdSO_4$ side phase. However, the spectrum coincides roughly with isotypic $M_4[B_2O(SO_4)_6]$ (M = Mn, Co, Ni, Zn) and the assigned bands given within the original publication.[8]
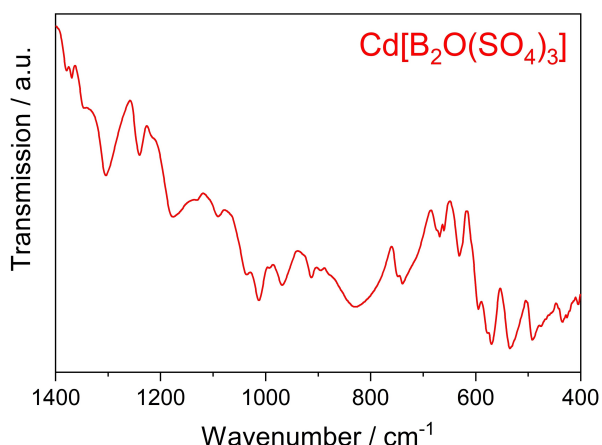
Figure 6. Infrared spectrum of Cd[B$_2$O(SO$_4$)$_3$]: The full spectrum can be found in Figure S6.

The **UV-Vis powder reflectance spectrum** of Cd[B$_2$O(SO$_4$)$_3$] was recorded. Since there are no valence d-orbital electrons in Cd^{2+}, it is dominated by the fundamental absorption due to the bandgap of the sample in the UV region. The optical band gap was estimated using the Tauc plot in Figure 7 assuming a direct band gap with an experimental value of 4.48(1) eV.

Thermal Analyses

In general, borosulfates decompose to the respective metal sulfates and amorphous boron oxide while releasing gaseous SO$_3$. Then, these decompose further to the respective metal oxides, which might react with the B$_2$O$_3$ to the respective metal borates. Moreover, the decomposition of a borosulfate yielding another was observed frequently. Here, the stability increases from S–O–S via B–O–S to B–O–B bridges containing borosulfates.[3,8,9,12,15,27] Since the title compounds were prepared by the thermal decomposition of the conventional borosulfate
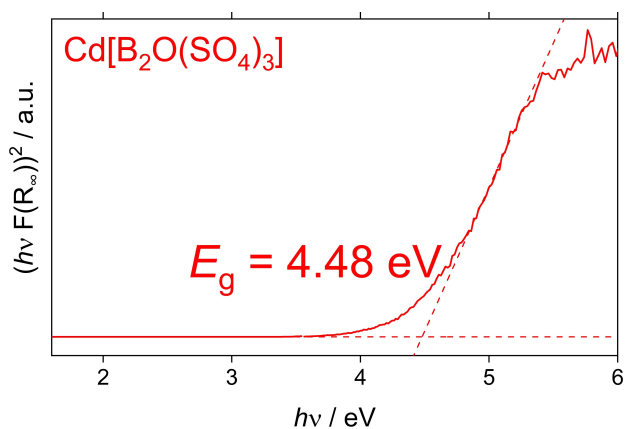
Cd[B$_2$(SO$_4$)$_4$] this provides a detailed case study of the complex thermal decomposition behaviour of such borosulfates.

Cd[B$_2$O(SO$_4$)$_3$] decomposes under nitrogen atmosphere via a two-step process to CdO and B$_2$O$_3$ with the intermediate CdSO$_4$. The experimentally observed and the expected mass losses agree very well for this process that is accompanied by evaporation of SO$_3$ (Figure 8). This is in line with the temperature-dependent powder XRD (TPXRD) depicted in Figure S9 confirming the formation of the intermediate. However, the previous characterisation of Cd$_4$[B$_2$O(SO$_4$)$_6$] indicates that this is not the whole story since this phase is expected to form prior to CdSO$_4$. Similarly, the thermogravimetry results on Cd[B$_2$(SO$_4$)$_4$] suggest a single step decomposition process to CdSO$_4$ – with no further intermediates.[16] However, both, Cd[B$_2$O(SO$_4$)$_3$] and Cd$_4$[B$_2$O(SO$_4$)$_6$], could be prepared by isothermal heating programs within this temperature regime. The main reason for these findings is probably not the presence of air during the syntheses of the title compounds (Figure S10), but the heating rate as well as the differences between dynamic, stepwise, and isothermal heating.

The pattern observed at 300 °C during the TPXRD of Cd[B$_2$(SO$_4$)$_4$] elsewhere[16] shows the formation of Cd[B$_2$O(SO$_4$)$_3$] (Figure S11). When heating Cd[B$_2$(SO$_4$)$_4$] slowly (1 K min^{-1}) two additional steps related to the formation of the two title compounds are found during TGA (Figure S12). However, the observed mass losses for these two steps occurring between 140 and 190 °C, and 250 and 310 °C, respectively, are smaller than expected indicating that the heating is still too fast for the underlying processes to occur completely. This issue is circumvented when heating Cd[B$_2$(SO$_4$)$_4$] in an open ampoule for several hours isothermally as done for the syntheses of the title compounds. Due to the hygroscopic nature of the samples the furnace was preheated to 150 °C prior to all treatments and the samples were taken out of the furnace at 150 °C at least – followed by immediate transfer into an argon filled glovebox. Besides the holding temperature, the temperature at which the sample was taken out of the furnace also showed an influence on the phase composition of the final sample. The cooling
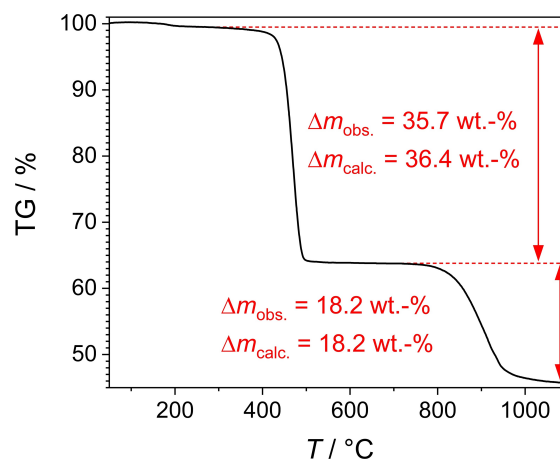

Figure 7. Tauc plot calculated from the UV-Vis spectrum of Cd[B$_2$O(SO$_4$)$_3$] displayed in Figure S8 assuming a direct band gap.

Figure 8. Thermogravimetric analysis of Cd[B$_2$O(SO$_4$)$_3$] with a 10 K·min^{-1} heating rate.

process can be described as quenching the sample at room temperature in ambient air for several seconds and in argon for several minutes. $Cd[B_2O(SO_4)_3]$ is prepared via isothermal heating of $Cd[B_2(SO_4)_4]$ at 250 °C (Figure 1). When heating $Cd[B_2(SO_4)_4]$ at 300 °C the cooling's influence becomes crucial. When the sample is quenched at 280 °C, a mixture of 89 wt.% $Cd_4[B_2O(SO_4)_6]$ and 11 wt.% $CdSO_4$ is formed (Figure S1) while quenching at 250 °C results in a phase mixture of two thirds $Cd_4[B_2O(SO_4)_6]$ and one third $Cd[B_2O(SO_4)_3]$ (Figure S13). Quenching at 150 °C leads to a 1:1 phase mixture of $Cd[B_2O(SO_4)_3]$ and $Cd_4[B_2O(SO_4)_6]$ (Figure S14). This indicates a certain reversibility of the reaction towards $Cd_4[B_2O(SO_4)_6]$ upon cooling. This is surprising because these reactions are expected to be accompanied by evaporation of SO_3. When heating at 350 °C or 400 °C, there is no influence of the cooling anymore. In all cases, $CdSO_4$ is formed (Figure S15).

Similar behaviour was reported for the three barium borosulfates $Ba[B(S_2O_7)_2]_2$, $Ba[B_2(SO_4)_4]$ and $Ba[B_2O(SO_4)_3]$. There, the decomposition of $Ba[B_2(SO_4)_4]$ towards $Ba[B_2O(SO_4)_3]$ could be only observed via TPXRD since this step was overlapped in the TG result by the subsequent decomposition towards $BaSO_4$.[12]

These findings point to the fact that the thermal decomposition behaviour of borosulfates is highly dependent on the heating program including the rate of both heating and cooling. Consequently, these are parameters that are worth investigating for other borosulfates. There are still several borosulfates whose thermal properties were not studied at all. But also, for the one with TGA results one should not expect their thermal properties to be fully understood in the light of the results presented herein.

Conclusions

In this contribution, the solvothermal syntheses, the crystal structures as well as the optical and thermal properties of the two unconventional cadmium borosulfates $Cd[B_2O(SO_4)_3]$ and $Cd_4[B_2O(SO_4)_6]$ – both comprising B–O–B bridges – were elucidated. Cadmium is the first metal for which both borosulfates with the sum formulae $M[B_2O(SO_4)_3]$ and $M_4[B_2O(SO_4)_6]$ were reported. This can be explained by the special position of cadmium within the periodic table and its according janiform behaviour. Further, the optical and thermal properties of both compounds were studied. The title compounds are thermal decomposition products of the conventional borosulfate $Cd[B_2(SO_4)_4]$. The complex thermal decomposition behaviour of this borosulfate was investigated in detail. It was shown that not only the heating and cooling rate but also the heating type (dynamic, stepwise, or isothermal) can play a crucial role in these processes. Consequently, it can be expected that many borosulfates have been overlooked in the past due to determining their thermal properties using e.g. a single heating rate only. Our results might enable new synthesis pathways for especially unconventional borosulfates comprising B–O–B bridges. For example, $Ca[B_2O(SO_4)_3]$[28] might be accessible this

way in order to elucidate its crystal structure and further properties.

Experimental Section

Syntheses

Firstly, $Cd[B_2(SO_4)_4]$ was prepared solvothermally – as detailed in Ref. 16. 0.5 mmol CdO (Fluka, 99 %) and 1.25 mmol B_2O_3 (Sigma–Aldrich, 99 %) were ground together, and filled into a silica glass ampoule (length 150 mm, outer diameter: 12 mm, wall thickness: 1 mm) together with 1 ml oleum (VWR, 65 % SO_3). Subsequently, the ampoule was fused under ambient pressure and placed in a muffle furnace applying the following temperature program: heating to 300 °C with 100 °C min^{-1}, holding the temperature for 60 h, and cooling down to room temperature with 100 °C min^{-1}.

Afterwards, the ampoule was flipped over in order to separate the sample from the excess sulfuric acid via decantation. Then, the ampoule was opened after cooling with liquid nitrogen (Caution: During and even after the reaction the ampoules are under remarkable pressure and must therefore be handled with care).

For the preparation of $Cd[B_2O(SO_4)_3]$, the open end containing the $Cd[B_2(SO_4)_4]$ sample was immediately transferred into a muffle furnace preheated to 150 °C. Then, it was heated at 250 °C for 24 h, cooled to 150 °C within 1 h and directly transferred to an argon filled glovebox. Both products are sensitive towards moisture and hence were stored under inert conditions for further investigations.

For $Cd_4[B_2O(SO_4)_6]$, the same procedure was followed. The temperature program after transferring the open end of the ampoule into the muffle furnace was changed to 2 h at 300 °C. Afterwards, the furnace was cooled naturally to 280 °C and the sample was taken out and directly transferred to the glovebox. Due to the quenching of the sample at air and argon, respectively, the separation of the final sample from the ampoule was complicated. Thus, only small sample quantities could be prepared this way. As a consequence, $Cd_4[B_2O(SO_4)_6]$ was characterised by PXRD and FTIR spectroscopy, only.

Single-Crystal X-Ray Structure Determination

Suitable single-crystals were embedded in perfluorinated polyether and selected for single-crystal XRD under a polarising microscope. Diffraction data were collected with a Bruker D8 Venture diffractometer using Mo-K$_\alpha$ radiation ($\lambda = 0.71073$ Å). Absorption correction was performed by the multiscan method. The structures were solved by Direct Methods and refined by full-matrix least-squares technique with the SHELXTL crystallographic software package.[29] Relevant crystallographic data and further details of the structure determinations are summarised in Tables 1 and S2–3. $Cd_4[B_2O(SO_4)_6]$ was refined as a two-component inversion twin (twin matrix: 1 0 0 0 1 0 0 0 −1; BASF: 0.58(1)). This type of twinning was also observed for other borosulfates adapting the structure type of α-$Mg_4[B_2O(SO_4)_6]$.[8]

Further details of the crystal structure investigations may be obtained at https://www.ccdc.cam.ac.uk/ on quoting the depository numbers CSD-CSD-2177539 ($Cd_4[B_2O(SO_4)_6]$) and 2177540 ($Cd[B_2O(SO_4)_3]$), the names of the authors, and citation of this publication.

Powder X-Ray Diffraction (PXRD)

The samples were ground and filled into a Hilgenberg glass capillaries (outer diameter 0.3 mm, wall thickness 0.01 mm) inside an argon filled glovebox. The data were collected with a Bruker D8 Advance diffractometer with Cu–Kα radiation ($\lambda = 1.54184$ Å) with a 1D LynxEye detector, steps of 0.02° and transmission geometry. The generator was driven at 40 kV and 40 mA. The background at lower diffraction angles is due to the absorption of the glass capillary.

Temperature-programmed X-Ray Powder Diffraction (TPXRD) was performed with the same device using a furnace attachment and a silica-glass Hilgenberg capillary (outer diameter 0.3 mm, wall thickness 0.01 mm). The background between $12.5° < 2\theta < 30°$ is due to the used furnace attachment.

Rietveld Refinement

Analysis of diffraction data was performed using the Rietveld method with the program TOPAS 5.[30] The instrumental resolution function was determined empirically from a set of fundamental parameters using a reference scan of Si (NIST 640d).[31] The structural models of $Cd[B_2O(SO_4)_3]$ and $Cd_4[B_2O(SO_4)_6]$ from our single-crystal XRD data and $CdSO_4$[32] were used as starting models for Rietveld analysis. The isotropic thermal displacement parameters were constrained to common values per atom type to minimise quantification errors. The background was modeled with a Chebychev polynomial. Details are displayed in Tables S1.

FTIR spectroscopy

The Fourier-transform infrared spectra were recorded at room temperature with a Bruker EQUINOX 55 T-R spectrometer using a Platinum ATR device (scan range: 400–4000 cm^{-1}, resolution: 2 cm^{-1}, 32 scans per sample).

UV-Vis Spectroscopy

The UV-Vis spectrum was recorded as diffuse reflection spectrum at room temperature with a Varian Cary 300 Scan UV-Vis spectrophotometer using an Ulbricht sphere detector and a deuterium lamp/tungsten-halogen lamp light source (scan range: 200–800 nm, increment 1 nm, scan rate: 120 nm min^{-1}).

Thermal Analysis

The thermogravimetric analysis (TGA) was performed with a NETZSCH STA 409 PC Luxx thermobalance under nitrogen or synthetic air atmosphere with 50 mL min^{-1} flow in alumina crucibles (heating rate – if not stated otherwise: 10 K·min^{-1}). Additional samples of $Cd[B_2(SO_4)_4]$ were heat treated in muffle furnaces. Details are found in the supporting information with the respective diffraction data.

Acknowledgements

Conflict of Interest

The authors declare no conflict of interest.

Data Availability Statement

The data that support the findings of this study are available from the corresponding author upon reasonable request.

[1] J. Bruns, H. A. Höppe, M. Daub, H. Hillebrecht, H. Huppertz, *Chem. Eur. J.* **2020**, *26*, 7966–7980.
[2] H. A. Höppe, K. Kazmierczak, M. Daub, K. Förg, F. Fuchs, H. Hillebrecht, *Angew. Chem. Int. Ed.* **2012**, *51*, 6255–6257; *Angew. Chem.* **2012**, *124*, 6359–6362.
[3] M. Hämmer, F. Pielnhofer, O. Janka, H. Takahashi, P. Gross, R. Pöttgen, H. A. Höppe, *Dalton Trans.* **2022**, *51*, 3104–3115.
[4] Z. Li, W. Jin, F. Zhang, Z. Chen, Z. Yang, S. Pan, *Angew. Chem. Int. Ed.* **2022**, *61*, e202112844.
[5] P. Netzsch, R. Stroh, F. Pielnhofer, I. Krossing, H. A. Höppe, *Angew. Chem. Int. Ed.* **2021**, *60*, 10643–10646; *Angew. Chem.* **2021**, *133*, 10738–10741.
[6] F. Liebau, *Structural Chemistry of Silicates*, Springer, Heidelberg **1985**.
[7] F. J. Pucher, F. W. Karau, J. Schmedt auf der Günne, W. Schnick, *Eur. J. Inorg. Chem.* **2016**, *2016*, 1497–1502.
[8] P. Netzsch, P. Gross, H. Takahashi, H. A. Höppe, *Inorg. Chem.* **2018**, *57*, 8530–8539.
[9] P. Netzsch, H. A. Höppe, *Inorg. Chem.* **2020**, *59*, 18102–18108.
[10] W. Loewenstein, *Amer. Min.* **1954**, *39*, 92–96.
[11] L. Pauling, *J. Am. Chem. Soc.* **1929**, *51*, 1010–1026.
[12] P. Netzsch, F. Pielnhofer, H. A. Höppe, *Inorg. Chem.* **2020**, *59*, 15180–15188.
[13] L. C. Pasqualini, H. Huppertz, M. Je, H. Choi, J. Bruns, *Angew. Chem. Int. Ed.* **2021**, *60*, 19740–19743; *Angew. Chem.* **2021**, *133*, 19892–19896.
[14] P. Gross, A. Kirchhain, H. A. Höppe, *Angew. Chem. Int. Ed.* **2016**, *55*, 4353–4355; *Angew. Chem.* **2016**, *128*, 4426–4428.
[15] P. Netzsch, P. Gross, H. Takahashi, S. Lotfi, J. Brgoch, H. A. Höppe, *Eur. J. Inorg. Chem.* **2019**, 3975–3981.
[16] M. Hämmer, L. C. Pasqualini, S. S. Sebastian, H. Huppertz, H. A. Höppe, J. Bruns, *Dalton Trans.* **2022**, accepted, DOI: 10.1039/D2DT02344J.
[17] L. C. Pasqualini, H. Huppertz, J. Bruns, *Inorganics* **2019**, *7*, 145.
[18] a) E. Carmona, A. Galindo, *Angew. Chem. Int. Ed.* **2008**, *47*, 6526–6536; *Angew. Chem.* **2008**, *120*, 6626–6637; b) W. B. Jensen, *J. Chem. Educ.* **2003**, *80*, 952.
[19] R. T. Sanderson, *J. Chem. Educ.* **1964**, *41*, 187.
[20] R. D. Shannon, *Acta Crystallogr. Sect. A* **1976**, *32*, 751–767.
[21] E. Makovicky, T. Balić-Žunić, *Acta Crystallogr.* **1998**, *B54*, 766–773.
[22] T. Balić Žunić, E. Makovicky, *Acta Crystallogr.* **1996**, *B52*, 78–81.
[23] H. A. Höppe, *J. Solid State Chem.* **2009**, *182*, 1786–1791.
[24] M. Daub, H. Hillebrecht, *Eur. J. Inorg. Chem.* **2015**, *2015*, 4176–4181.
[25] F. Stadler, O. Oeckler, J. Senker, H. A. Höppe, P. Kroll, W. Schnick, *Angew. Chem. Int. Ed.* **2005**, *44*, 567–570; *Angew. Chem.* **2005**, *117*, 573–576.
[26] a) R. Hübenthal, *MAPLE. Program for the Calculation of the Madelung Part of Lattice Energy*, Universität Gießen, Gießen

1993; b) R. Hoppe, *Z. Kristallogr.* **1979**, *150*, 23–52; c) R. Hoppe, *Angew. Chem. Int. Ed.* **1970**, *9*, 25–34; *Angew. Chem.* **1970**, *82*, 7–16; d) R. Hoppe, *Angew. Chem.* **1966**, *78*, 52–63; *Angew. Chem. Int. Ed.* **1966**, *5*, 95–106.

[27] a) M. Hämmer, L. Bayarjargal, H. A. Höppe, *Angew. Chem. Int. Ed.* **2021**, *60*, 1503–1506; *Angew. Chem.* **2021**, *133*, 1525–1529; b) P. Netzsch, M. Hämmer, P. Gross, H. Bariss, T. Block, L. Heletta, R. Pöttgen, J. Bruns, H. Huppertz, H. A. Höppe, *Dalton Trans.* **2019**, *48*, 4387–4397.

[28] G. Schott, H. U. Kibbel, *Z. Anorg. Allg. Chem.* **1962**, *314*, 104–112.

[29] G. M. Sheldrick, *Acta Crystallogr. Sect. C* **2015**, *71*, 3–8.

[30] Bruker AXS, *Topas V5, General profile and structure analysis software for powder diffraction data. User's Manual*, Karlsruhe, Germany **2014**.

[31] R. W. Cheary, A. A. Coelho, J. P. Cline, *J. Res. Natl. Inst. Stand. Technol.* **2004**, *109*, 1–25.

[32] K. Aurivillius, C. Stålhandske, *Z. Kristallogr.* **1980**, *153*, 121–129.

RESEARCH ARTICLE

Cd$_4$[B$_2$O(SO$_4$)$_6$]   Cd[B$_2$O(SO$_4$)$_3$]   Cd[B$_2$(SO$_4$)$_4$]

0D   1D   2D
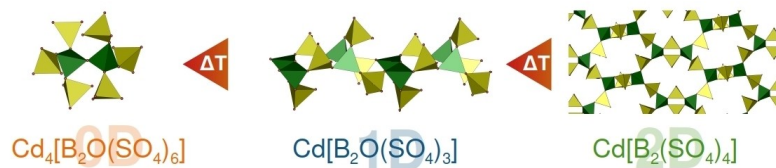
*Dr. M. Hämmer, Prof. Dr. H. A. Höppe***

1 – 9

The Unconventional Cadmium Borosulfates Cd[B$_2$O(SO$_4$)$_3$] and Cd$_4$[B$_2$O(SO$_4$)$_6$]